

Sliding-Mode Observer-Based Mechanical Parameter Estimation for Permanent Magnet Synchronous Motor

Xiaoguang Zhang and Zhengxi Li, *Senior Member, IEEE*

Abstract—A mechanical parameter estimation algorithm for permanent magnet synchronous motor (PMSM) drive systems based on sliding-mode observer is proposed in this paper. First, an extended sliding-mode mechanical parameter observer (ESMMPO) is presented to track system disturbances in real time, which include the information of mechanical parameters. Based on this ESMMPO, the mechanical parameter can be extracted from the estimated system disturbance. Therefore, a simple algorithm for mechanical parameter estimation of the PMSM control system is presented. The parameter choice guidelines of ESMMPO are designed to guarantee the global stability of the observer. Then, the equivalent low-pass filter function of the ESMMPO is presented to suppress the sliding-mode chattering, which allows softening the output signal of observer while maintaining no phase lag incurring. Therefore, the smooth output of the ESMMPO can be directly used for the parameter estimation. Experimental results show the validity of the proposed parameter estimation approach.

Index Terms—Extended state, parameter estimation, permanent magnet synchronous motor (PMSM), sliding-mode observer (SMO).

I. INTRODUCTION

PERMANENT magnet synchronous machines (PMSMs) are now widely used in many applications, ranging from electric vehicle, industrial drives, and wind power generation to aerospace, due to their high precision, high efficiency, high speed, high reliability, and excellent control performance. In a high-performance control system of PMSM, parameter accuracy is an important factor that influences control precision of the whole system. Especially, mechanical parameters, including the moment of inertia of the whole system, the viscous damping coefficient, and the load torque, play a key role in achieving high dynamic performance of the speed control. If these parameters can be estimated accurately, the autotuned controller of PMSM systems can be achieved easily, which means optimal control

Manuscript received November 17, 2014; revised June 22, 2015 and August 19, 2015; accepted October 21, 2015. Date of publication October 27, 2015; date of current version March 2, 2016. This work was supported in part by the National Natural Science Foundation of China under Grant 51507004, by the Natural Science Foundation of Beijing under Grant 4152013, by the Scientific Research Foundation for the Returned Overseas Chinese Scholars, by Beijing City and the Scientific Research Foundation of North China University of Technology. Recommended for publication by Associate Editor Y. Sozer.

The authors are with Power Electronics and Motor Drives Engineering Research Center of Beijing, North China University of Technology, Beijing 100144, China, and also with the Collaborative Innovation Center of Electric Vehicles in Beijing (e-mail: zxg@ncut.edu.cn; lzx@ncut.edu.cn).

Color versions of one or more of the figures in this paper are available online at <http://ieeexplore.ieee.org>.

Digital Object Identifier 10.1109/TPEL.2015.2495183

method can be designed to improve the control performance of the PMSM systems.

Therefore, many parameter estimation methods have been proposed, and basically can be categorized into five groups: parameter adaptation [1]–[5], model reference adaptive system (MRAS) [6]–[11], recursive least squares (RLS)[7]–[8], observer-based methods, and extended Kalman filter (EKF) [9]–[13]. The MRAS-based method is simple and easy to implement, which has been used for estimating parameter in many applications [14]–[18]. However, this method cannot be applied for estimating the load torque in real time. Parameter adaptation method can be used for estimating parameter by adjusting adaptive law or function cost continuously. However, it is difficult for real application because of the complexity in practical implementation and the sensitivity of adaptation gains. EKF algorithm treats mechanical parameter as one of the system variables, and such estimates are obtained as a direct output of the EKF, while RLS iteratively solves the least squares estimates upon convergence which relatively much depends on initial conditions. Although RLS method can be applied for estimating the parameter of a PMSM control system, it requires a long estimated time and a special trajectory of reference velocity during the estimation. Therefore, this method is limited in some practical applications [4], [19].

Observer-based approaches, including disturbance observer (DOB) and sliding-mode observer (SMO), are attracting widespread interest because its design and implementation is relatively simple for parameter estimation. The DOB method can be applied for estimating viscous friction coefficient, rotational inertia, and load disturbances by means of building disturbance estimators [20]–[23]. In [20], a state and load torque observer is developed to observe the unknown load torque in real time. In [23], a state observer for estimating motor disturbance and mechanical parameters is presented. In this method, two adaptive controllers following the state estimator are used to separately adjust the drive inertia and friction to their correct value. Although the DOB methods in [20] and [23] can achieve good performance and are able to estimate the mechanical parameters accurately, both of them have poor robustness. Compared to the DOB method, SMO has attractive advantages of robustness to disturbances and low sensitivity to the parameter variations of the whole system. Therefore, many SMO-based parameter estimation methods have been proposed. In [24], a novel SMO is designed to estimate the friction state of the LuGer model. In [25] and [26], in order to improve the estimation accuracy, the second-order SMO is designed for the identification

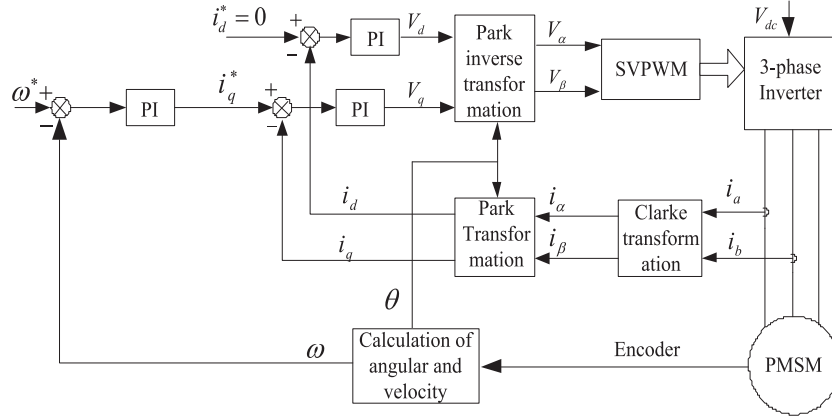


Fig. 1. Structure diagram of the PMSM vector control system.

of mechanical systems. However, in aforementioned observers, the low-pass filter (LPF) must be used to obtain the estimated parameters, which will lead to the phase lag and the amplitude attenuation, then reduce the estimation accuracy.

In this paper, an extended SMO-based method for estimating the mechanical parameters of the PMSM drive system is proposed. First, the system disturbances, which include parameter error of viscous friction coefficient, parameter error of rotational inertia, and load disturbances, are regarded as extended system state to build the extended state equation, which is used to design the extended sliding-mode mechanical parameter observer (ESMMPO). Based on the proposed ESMMPO, a simple algorithm for mechanical parameter estimation of the PMSM control system is developed. This ESMMPO can track system states in real time, and can be equivalent to an LPF, which can soften switching control signal of the sliding mode. Therefore, the output of the ESMMPO can be directly used for the mechanical parameter estimation with no phase lag incurring. Finally, the effectiveness of the proposed parameter estimation approach was verified by experimental results.

II. MACHINE MODEL

Assuming that the employed SPMSM has negligible cross-coupling magnetic saturation, structural asymmetry, iron losses, magnet eddy current loss, and harmonics in the descriptive functions of windings, rotor anisotropy, and coercive force of magnets, the dynamics of a SPMSM in the rotor *d*-*q* coordinates can be described as follows [27]:

$$\begin{cases} u_d = Ri_d - p\omega Li_q + L\dot{i}_d \\ u_q = Ri_q + p\omega Li_d + p\omega\Psi_a + L\dot{i}_q \end{cases} \quad (1)$$

$$T_e = 1.5p\Psi_a i_q \quad (2)$$

$$T_e - T_L = J\ddot{\omega} + B\omega \quad (3)$$

where u_d and u_q represent *d*- and *q*-axis stator voltages; i_d and i_q are *d*- and *q*-axis currents; L is the stator inductance; R is the stator winding resistance; T_e is the electrical magnetic torque ($N\cdot m$); T_L is the load torque ($N\cdot m$); p is the number of pole pairs; Ψ_a is the flux linkage of permanent magnets; ω is the angular

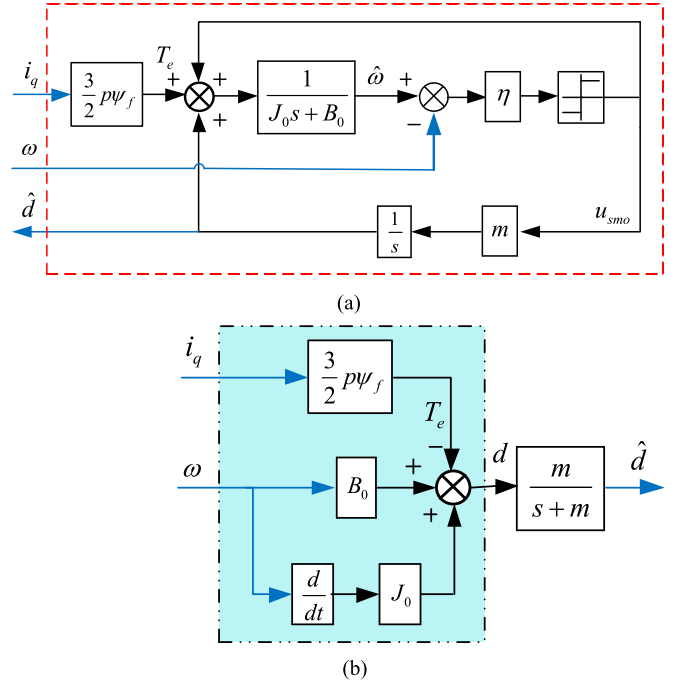


Fig. 2. Schematic block diagram of the ESMMPO and equivalent LPF. (a) ESMMPO. (b) Equivalent LPF after sliding mode occurring.

TABLE I
PARAMETERS OF PMSM CONTROL SYSTEM

<i>d</i> - and <i>q</i> -axes inductances	$L_d = L_q = 9 \text{ mH}$
Stator phase resistance	$R = 2.6 \Omega$
Viscous friction coefficient	$B = 0.003 \text{ N}\cdot\text{m}\cdot\text{s}/\text{rad}$
Number of pole pairs	$P = 4$
Rotational inertia	$J = 0.0102 \text{ kg}\cdot\text{m}^2$
Flux linkage of permanent magnets	$\Psi_a = 0.175 \text{ Wb}$

velocity (rad/s); B is the viscous friction coefficient; and J is the rotational inertia ($\text{kg}\cdot\text{m}^2$).

Typical structure diagram of the PMSM vector control system is shown as Fig. 1. The power part is comprised of the PWM voltage source inverter and PMSM. The stator currents and motor speed can be directly measured by current sensors and position encoder, respectively. The control parts employ a structure of cascade control loops including a speed loop and

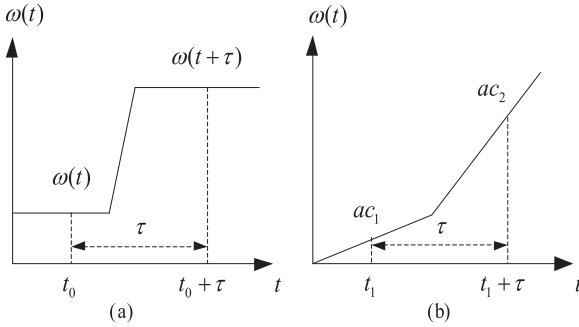


Fig. 3. Principle diagram of mechanical parameter estimation. (a) Estimating B . (b) Estimating J .

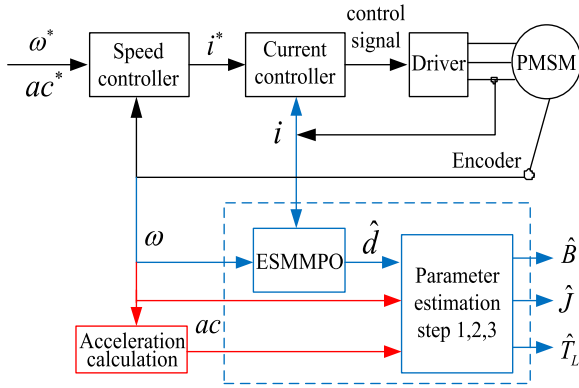


Fig. 4. Structure diagram of the parameter estimation.



Fig. 5. Photograph of the experimental setup.

two current loops, i.e., speed outer loop and two current inner loops. The current inner loop is comprised of d -axis control loop and q -axis control loop, which can be used to control the d -axis and q -axis current (i_d and i_q), respectively. The currents i_d and i_q can be calculated from i_a and i_b (which can be measured by current sensors) by Clarke and Park transformations. Usually, the reference current i_d^* and i_q^* are set to be zero and output of speed loop, respectively. Moreover, the outputs of d -axis and q -

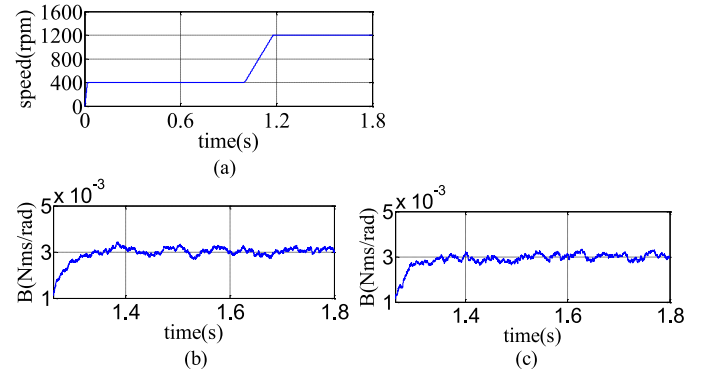


Fig. 6. Simulation results of estimated B under positive speed state. (a) Measured speed. (b) $B_0 = 0.0001 B$. (c) $B_0 = 50 B$.

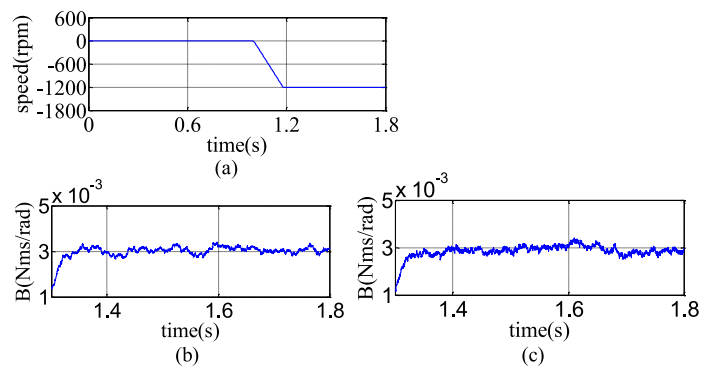


Fig. 7. Simulation results of estimated B under zero speed and speed reversals. (a) Measured speed. (b) $B_0 = 0.0001 B$. (c) $B_0 = 50 B$.

axis current loop are used to generate the drive signal of inverter by Park inverse transformations and space vector pulse width modulation (SVPWM).

Generally, the PI controller in speed loop and the PI controller in current loop, as shown as Fig. 1, are designed based on (1) and (3), which represent the PMSM electrical model and mechanical model, respectively. Therefore, the parameter accuracy of both the electrical and mechanical models is very important for controller design in a PMSM system. The electrical model (1) includes parameter R , L , p , and Ψ_a , which can be expressed as electrical parameters. The mechanical model (3) includes parameter B , J , and T_L , which can be expressed as mechanical parameters. The mechanical parameters of a PMSM system are unmeasurable but play a key role in the controller design of speed loop, which will determine both the dynamical and steady-state performances of a PMSM system. However, compared with the mechanical parameters, the electrical parameters can be easily measured using instruments or sensors. Therefore, this paper focuses on the estimation of the mechanical parameters J , B , and T_L .

III. EXTENDED SLIDING-MODE MECHANICAL PARAMETER OBSERVER

According to (3), the dynamic equation of the motor can be expressed as follows, with the system disturbances taken into

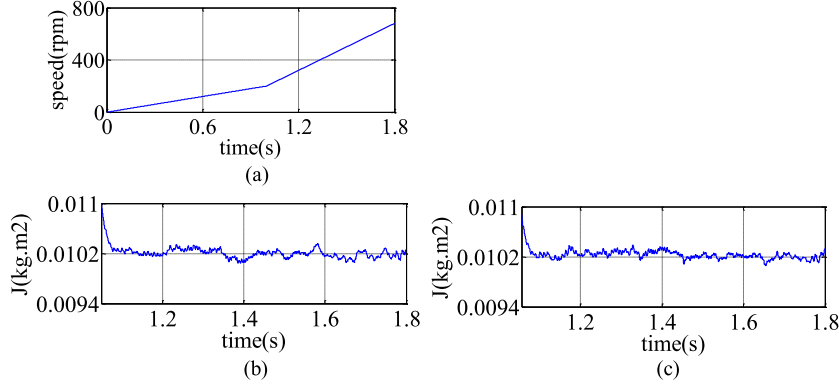


Fig. 8. Simulation results of estimated J under positive acceleration state. (a) Measured speed. (b) $J_0 = 0.001 J$. (c) $J_0 = 10 J$.

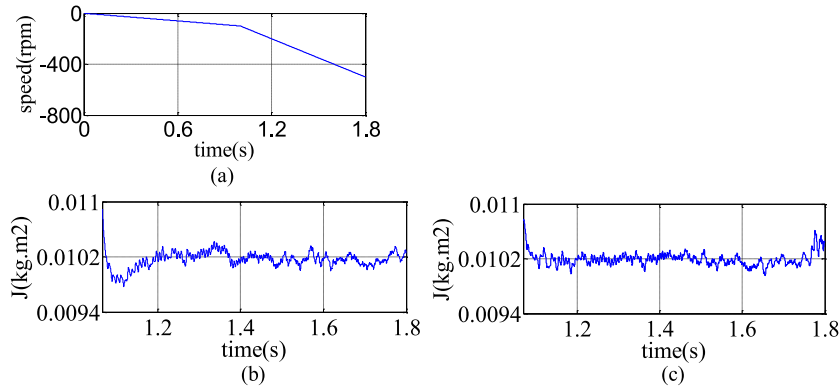


Fig. 9. Simulation results of estimated J under acceleration reversals. (a) Measured speed. (b) $J_0 = 0.001 J$. (c) $J_0 = 10 J$.

account:

$$J_0 \dot{\omega} = T_e - B_0 \omega + d \quad (4)$$

where $J = J_0 + \Delta J$ and $B = B_0 + \Delta B$. B_0 and J_0 are crude estimations of the true parameters, which can be determined initially based on the experiences and prior knowledge. ΔJ and ΔB are parameter errors between the true system and their crude estimations.

In (4), d represents the disturbances including parameter errors and load disturbances, i.e.,

$$d = -\Delta J \dot{\omega} - \Delta B \omega - T_L. \quad (5)$$

Furthermore, disturbances d are regarded as an extended system state, and then dynamic model (4) can be rewritten as the following extended state equation:

$$\begin{cases} J_0 \dot{\omega} = T_e - B_0 \omega + d \\ \dot{d} = r \end{cases} \quad (6)$$

where r is the variation rate of system disturbances d . According to (5), r can be described as $r = -\Delta J \ddot{\omega} - \Delta B \dot{\omega} - \dot{T}_L$.

For the purpose of parameter estimation, the ESMMPO can be designed as

$$\begin{cases} J_0 \dot{\hat{\omega}} = T_e - B_0 \hat{\omega} + \hat{d} + u_{smo} \\ \dot{\hat{d}} = mu_{smo} \end{cases} \quad (7)$$

where \hat{d} is an estimate of disturbances d , $\hat{\omega}$ is an estimate of speed ω , m is the sliding-mode parameter which is discussed in next section, and u_{smo} represents the SMO signal that is designed as

$$u_{smo} = \eta \cdot \text{sgn}(S) \quad (8)$$

where η is negative and S is the sliding-mode surface, which is designed as $S = \hat{\omega} - \omega$.

From (6) and (7), the error equation can be obtained as

$$\begin{cases} J_0 \dot{\hat{\omega}} - J_0 \dot{\omega} = B_0 \hat{\omega} + \hat{d} - d + u_{smo} \\ \dot{\hat{d}} - \dot{d} = mu_{smo} - r. \end{cases} \quad (9)$$

Define $e_1 = \hat{\omega} - \omega$ and $e_2 = \hat{d} - d$. Then, (9) can be rewritten as

$$\begin{cases} J_0 \dot{e}_1 = -B_0 e_1 + e_2 + u_{smo} \\ \dot{e}_2 = mu_{smo} - r. \end{cases} \quad (10)$$

Based on the above descriptions and discussions, the parameter choice guidelines of ESMMPO and sliding-mode chattering suppression analysis are introduced as follows.

A. Choice of Observer Parameter

In order to ensure the sliding mode occurring, parameter η of observer should be selected reasonably, which means the stability condition of SMO must be satisfied. Therefore, the following Lyapunov function is considered: $V = 0.5 s^2$. Differentiating V with respect to time t gives

$$\dot{V} = s \cdot \dot{s} = e_1 \cdot \dot{e}_1. \quad (11)$$

From (10), (11) can be rewritten as

$$\begin{aligned} \dot{V} &= \frac{1}{J_0} e_1 (-B_0 e_1 + e_2 + u_{\text{smo}}) \\ &= \frac{1}{J_0} e_1 [(e_2 - B_0 e_1) + \eta \cdot \text{sgn}(e_1)] \\ &= \begin{cases} \frac{1}{J_0} e_1 [(e_2 - B_0 e_1) + \eta], & e_1 > 0 \\ \frac{1}{J_0} e_1 [(e_2 - B_0 e_1) - \eta], & e_1 < 0. \end{cases} \end{aligned} \quad (12)$$

To ensure the stability of ESMMPO, stability condition $\dot{V} = s \cdot \dot{s} = e_1 \cdot \dot{e}_1 < 0$ must be satisfied, then (12) can be expressed as

$$\dot{V} = \begin{cases} \frac{1}{J_0} e_1 [(e_2 - B_0 e_1) + \eta], & e_1 > 0 \\ \frac{1}{J_0} e_1 [(e_2 - B_0 e_1) - \eta], & e_1 < 0 \end{cases} < 0. \quad (13)$$

As a result,

$$\eta < -|e_2 - B_0 e_1|. \quad (14)$$

Relation (13) and (14) show that in order to ensure the observer stability, the selection of parameter η need to meet the limiting condition. In practical application, the following parameter adaptive law can be used:

$$\eta = -l |e_2 - B_0 e_1|, \quad l > 1 \quad (15)$$

where l is a safety factor of the sliding mode. Usually, $l = 2$ is enough to ensure the observer stability.

It can be seen that error e_1 and its derivative \dot{e}_1 can converge to zero along the sliding mode occurring in finite time, which means $e_1 = \dot{e}_1 = 0$. Therefore, error (10) can be simplified as

$$\begin{cases} e_2 = -u_{\text{smo}} \\ \dot{e}_2 = mu_{\text{smo}} - r \end{cases} \quad (16)$$

which can also be rewritten as

$$\dot{e}_2 + me_2 + r = 0. \quad (17)$$

Thus, the solution for e_2 can be obtained as

$$e_2 = e^{-mt} [C + \int r \cdot e^{mt} dt] \quad (18)$$

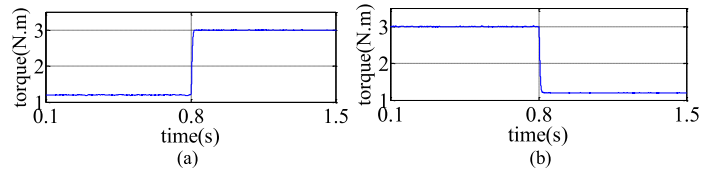


Fig. 10. Simulation results of estimated T_L . (a) Estimated load torque in case of sudden load increase from 1.2 to 3 N.m. (b) Estimated load torque in case of sudden load decrease from 3 to 1.2 N.m.

where C is a constant. To ensure that the disturbance estimation error e_2 converges to zero, the sliding-mode parameter is selected as

$$m > 0. \quad (19)$$

Moreover, the convergence rate of error e_2 is in direct relation with parameter m .

In the above analysis, general ideas about the role of the ESMMPO parameters and the way they can be chosen in the observer design are discussed. It can be seen that the choice of the ESMMPO parameters is only constrained by relations (14) and (19). The schematic block diagram of the ESMMPO is shown in Fig. 2.

B. Equivalent LPF Analysis

Speed can be described as $\omega = \hat{\omega}$ after sliding mode occurring. Then, (7) can be simplified as

$$\begin{cases} J_0 \dot{\hat{\omega}} = T_e - B_0 \omega + \hat{d} + u_{\text{smo}} \\ \dot{\hat{d}} = mu_{\text{smo}}. \end{cases} \quad (20)$$

Then, based on (6), the following equation can be obtained:

$$\dot{\hat{d}} + md\hat{d} = md. \quad (21)$$

Equation (21) is equivalent to the LPF, whose transfer functions $F(s)$ are given as follows:

$$\hat{d} = \frac{m}{s+m} \cdot d. \quad (22)$$

It can be seen that the disturbance observation effect of ESMMPO is equivalent to the output of filtering real-system disturbance. The cutoff frequency of the LPF is m , which can be designed arbitrarily based on the requirement of chattering suppression in the observer, since the condition (19) is satisfied (the effect of cutoff frequency on the performance of parameter estimation is discussed in Section V.). Thus, output of the proposed observer does not include the sliding-mode chattering because of the LPF and can be directly used for the system control.

According to above analysis, the proposed ESMMPO can be equivalent to an LPF after sliding mode occurring, then the schematic block diagram of the ESMMPO shown in Fig. 2(a) can be simplified as (b), which shows the schematic block diagram of an equivalent LPF.

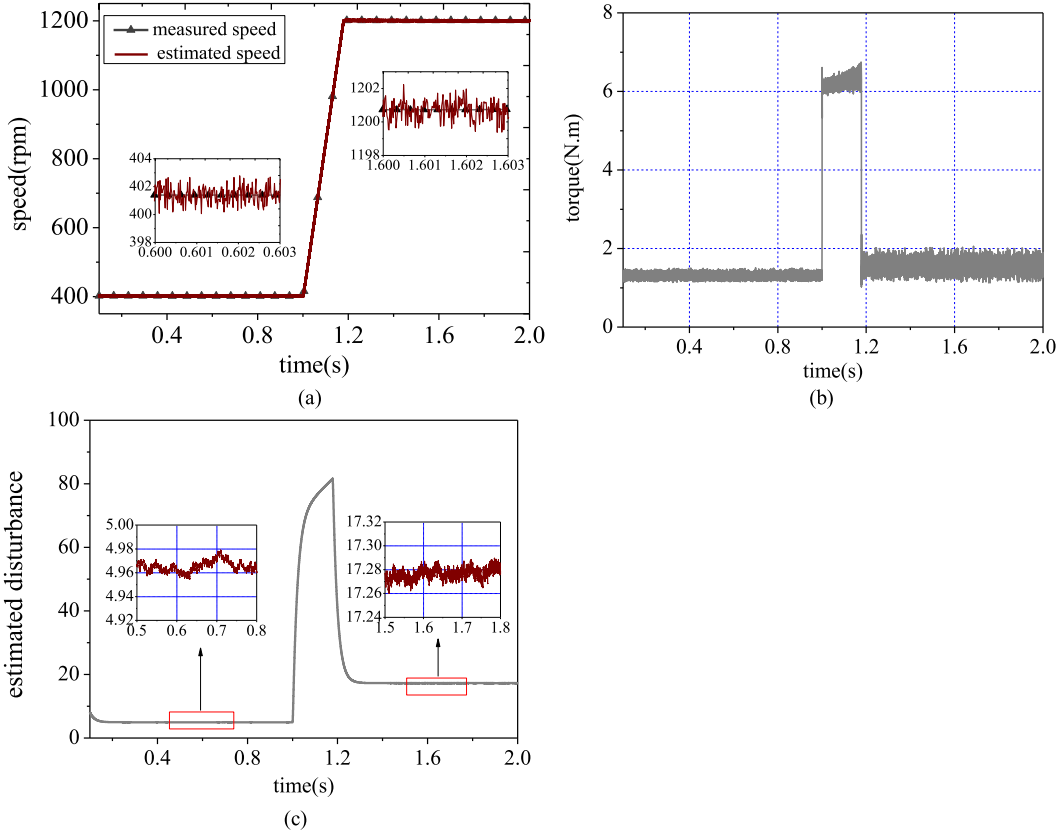


Fig. 11. Experimental results when estimating B . (a) Measured speed and estimated speed. (b) Torque. (c) Estimated disturbance in the case of $B_0 = 50 B$.

IV. PARAMETER ESTIMATION SCHEME

According to above analysis, it can be find that the proposed ESMMPPO can observe real-time information of system disturbances, which include mechanical parameters of the PMSM control system, at the same time, inherent chattering phenomenon of the sliding mode can be suppressed effectively. Therefore, the mechanical parameters can be extracted from the estimated system disturbance.

The estimation principle is shown in Fig. 3 and can be described as follows: First, at the stage of estimating B , as shown in Fig. 3(a), PMSM should be operated at two different steady velocities, and only measured velocity information and estimated disturbances are used for estimating parameter B during this stage. Second, at the stage of estimating J , as shown in Fig. 3(b), PMSM should be operated at two different constant accelerations or decelerations, respectively, and only accelerations or decelerations and estimated disturbances are used for estimating parameter J during this stage. Finally, after estimating B and J , estimated parameters are required to update to (5), which can be used to estimate load torque T_L directly.

However, it should be noted that before parameter estimation, optimal PI speed controller cannot be obtained because exact parameters B , J , and T_L are unknown. Therefore, the trial-and-error method-based nonoptimal PI speed controller can be used for mechanical parameter estimation. Obviously, good performance of the PMSM system cannot be obtained using this speed controller. However, since the parameter estimation method needs only the steady-state information of the system,

the nonoptimal PI controller has little effect on the parameter estimation.

Based on ESMMPPO, (4) and (5), the following method is proposed for mechanical parameters estimation in the PMSM system. The structure diagram of parameter estimation is shown as Fig. 4.

A. Step 1: Estimation of Parameter B

According to (4) and (5), estimated parameter B can be expressed as $\hat{B} = B_0 + \Delta\hat{B}$. Therefore, one can estimate \hat{B} by estimating parameter error $\Delta\hat{B}$ because crude estimation of parameter B_0 is known. When estimating B , as shown in Fig. 3(a), PMSM is required to operate at two different steady speeds, which satisfying $\omega(t) \neq \omega(t + \tau)$ and $\dot{\omega}(t) = \dot{\omega}(t + \tau) = 0$. In Fig. 3, τ is a constant time delay, which means that two different steady speeds correspond to two different periods of time, respectively. The value of τ is 1 s, and τ has no effect on the performance of parameter estimation.

When the motor operating at the first steady speed $\omega(t)$, based on ESMMPPO and (5), the disturbance estimation can be obtained as

$$\hat{d}(t) = -\Delta\hat{J}\dot{\omega}(t) - \Delta\hat{B}\omega(t) - T_L. \quad (23)$$

Then, delaying (23) by a time delay τ , the disturbance estimation for the second steady speed $\omega(t + \tau)$ is given as follows:

$$\hat{d}(t + \tau) = -\Delta\hat{J}\dot{\omega}(t + \tau) - \Delta\hat{B}\omega(t + \tau) - T_L. \quad (24)$$

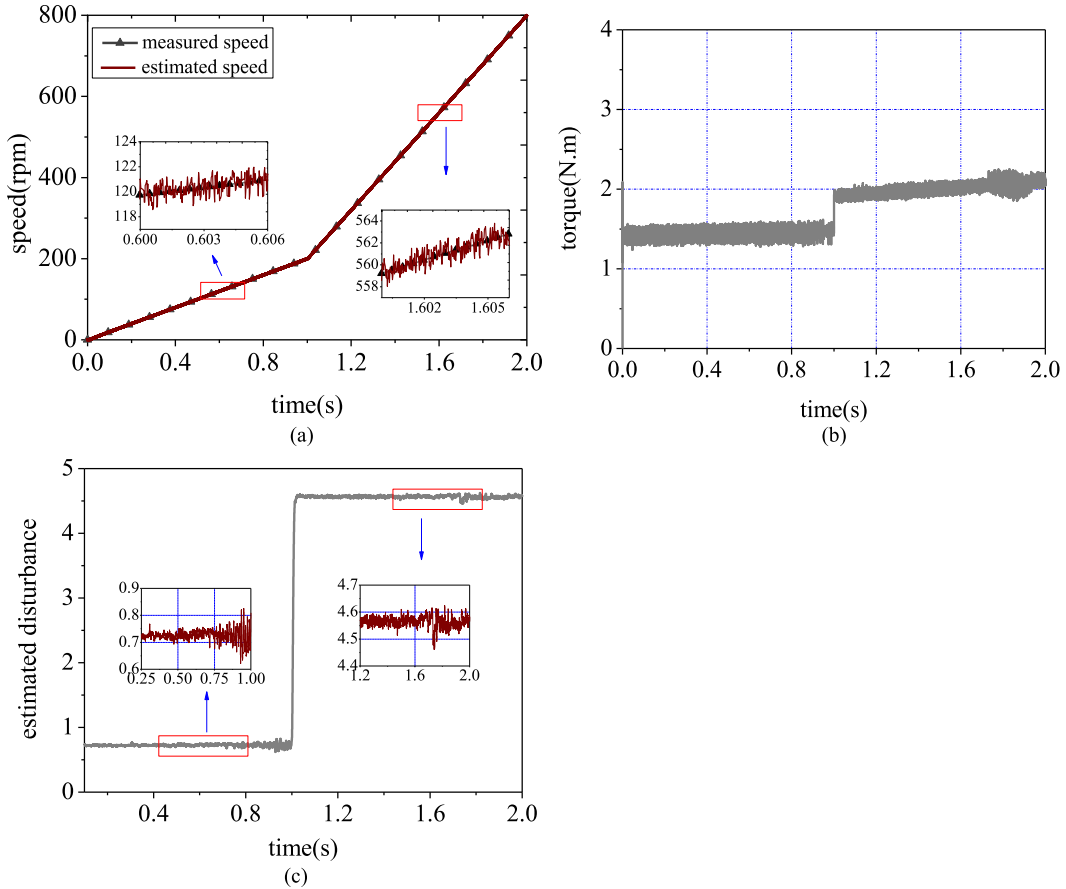


Fig. 12. Experimental results when estimating J . (a) Measured speed and estimated speed. (b) Torque. (c) Estimated disturbance in the case of $J_0 = 10 J$.

When the PMSM control system reaches its steady-state speed, load torque T_L can be considered as a constant. Then, subtracting (23) from (24) gives

$$\hat{d}(t + \tau) - \hat{d}(t) = -\Delta \hat{B}[\omega(t + \tau) - \omega(t)]. \quad (25)$$

Thus, $\Delta \hat{B}$ can be obtained as

$$\Delta \hat{B} = -\frac{\hat{d}(t + \tau) - \hat{d}(t)}{\omega(t + \tau) - \omega(t)}. \quad (26)$$

Therefore, estimated parameter \hat{B} can be obtained as follows:

$$\hat{B} = B_0 + \Delta \hat{B} = B_0 - \frac{\hat{d}(t + \tau) - \hat{d}(t)}{\omega(t + \tau) - \omega(t)}. \quad (27)$$

B. Step 2: Estimation of Parameter J

After estimating B , crude estimation B_0 in (7) can be updated by \hat{B} . Then, according to (5) and (7), disturbance estimation \hat{d} can be rewritten as

$$\hat{d} = -\Delta \hat{J} \dot{\omega} - T_L. \quad (28)$$

When estimating J , as shown in Fig. 3(b), the motor need to operate at the first constant acceleration state ac_1 . In this case, based on ESMMPO and (5), the disturbance estimation can be obtained as

$$\hat{d}(t) = -\Delta \hat{J} \cdot ac_1 - T_L. \quad (29)$$

Then, delaying (29) by a time delay τ , which ensure two different constant accelerations correspond to two different periods of time, respectively, the disturbance estimation for the second constant acceleration state ac_2 is given as follows:

$$\hat{d}(t + \tau) = -\Delta \hat{J} \cdot ac_2 - T_L. \quad (30)$$

Subtracting (30) from (29) gives

$$\hat{d}(t + \tau) - \hat{d}(t) = -\Delta \hat{J}(ac_2 - ac_1). \quad (31)$$

Thus, $\Delta \hat{J}$ can be obtained as

$$\Delta \hat{J} = -\frac{\hat{d}(t + \tau) - \hat{d}(t)}{ac_2 - ac_1}. \quad (32)$$

Therefore, estimated parameter \hat{J} can be obtained as follows:

$$\hat{J} = J_0 + \Delta \hat{J} = J_0 - \frac{\hat{d}(t + \tau) - \hat{d}(t)}{ac_2 - ac_1}. \quad (33)$$

In a practical PMSM control system, there exist load disturbances, which may vary as operation conditions vary. The control performance of a PMSM system will reduce seriously, if load disturbance cannot be suppressed effectively. Especially, it will be very difficult to limit load disturbances rapidly if adopting linear control algorithms like PI control method [27]. Therefore, in order to achieve excellent performance, it is very important for the PMSM control system to estimate load torque in real time.

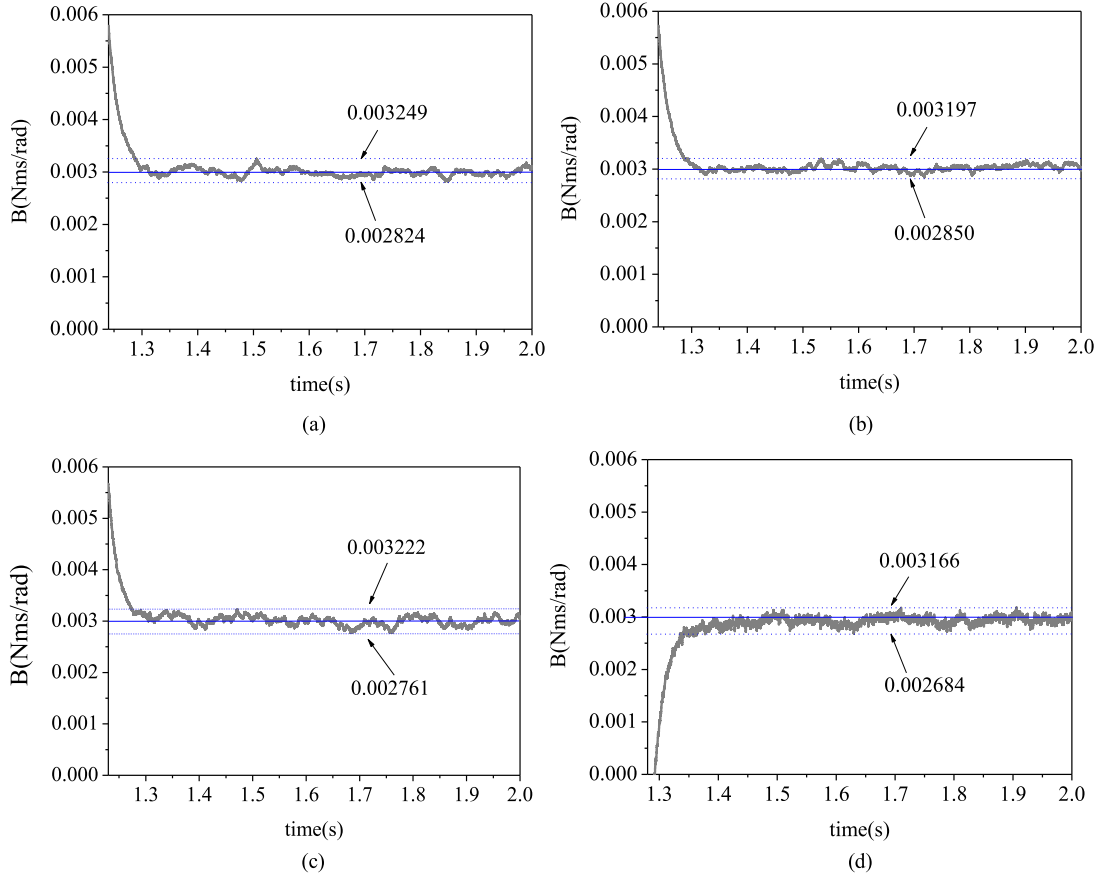


Fig. 13. Experimental results of estimated B . (a) $B_0 = 0.0001 B$. (b) $B_0 = 0.01 B$. (c) $B_0 = 1.33 B$. (d) $B_0 = 50 B$.

C. Step 3: Estimation of Load Torque T_L

When the parameters B and J is estimated accurately, crude estimation B_0 and J_0 in (7) can be replaced by estimated parameters, i.e., $\Delta J = J - \hat{J} = 0$ and $\Delta B = B - \hat{B} = 0$. Then, the ESMMPO (7) can be rewritten as

$$\begin{cases} \hat{J}\dot{\omega} = T_e - \hat{B}\dot{\omega} + \hat{d} + u_{smo} \\ \dot{\hat{d}} = mu_{smo} \end{cases} \quad (34)$$

where the updated disturbance estimation \hat{d} can be expressed as

$$\hat{d} = -T_L. \quad (35)$$

From (34) and (35), it can be seen that the updated ESMMPO have the ability of estimating load torque. Therefore, in practical application, the proposed ESMMPO can be used for estimating B and J , and can also be used for online real-time estimating load torque T_L when parameters B and J are known.

According to aforementioned parameter estimation step, it can be observed that the proposed method is simple and easy to implement. Moreover, this method does not need bidirectional rotating operation, thus it can be very useful, especially in the control system such that only the unidirectional rotation is allowed. The structure diagram of this parameter estimation method is shown in Fig. 4.

V. SIMULATION AND EXPERIMENTAL RESULTS

In this section, to evaluate the performance of the proposed parameter estimation approach, the simulation and experimental system for speed control of PMSM was built. Simulations are established in MATLAB/Simulink. The experiments platform is constructed by TMS320LF2812 processor and the system sampling frequency is 10 kHz. The photograph of the experimental setup including the PMSM, the motor drive, the load motor, and the control PC are shown in Fig. 5. In addition, the parameters of PMSM used in the experiment are listed in Table I.

The simulation results of the estimated B with different speed conditions are shown in Figs. 6 and 7. From the simulation results, it can be observed that the proposed method can estimate parameter B exactly when different speed conditions are utilized. Moreover, the simulation results of estimated J with different accelerations are shown in Figs. 8 and 9. When acceleration state is positive, the estimated parameter J can converge to the true value; on the other hand, the similar results also can be obtained when acceleration state is negative. In addition, estimated load disturbances are shown in Fig. 10, when load torque T_L is increased suddenly from 1.2 to 3 N·m and decreased from 3 to 1.2 N·m, respectively. It can be observed that the observer can estimate the load disturbance exactly and quickly with low chattering.

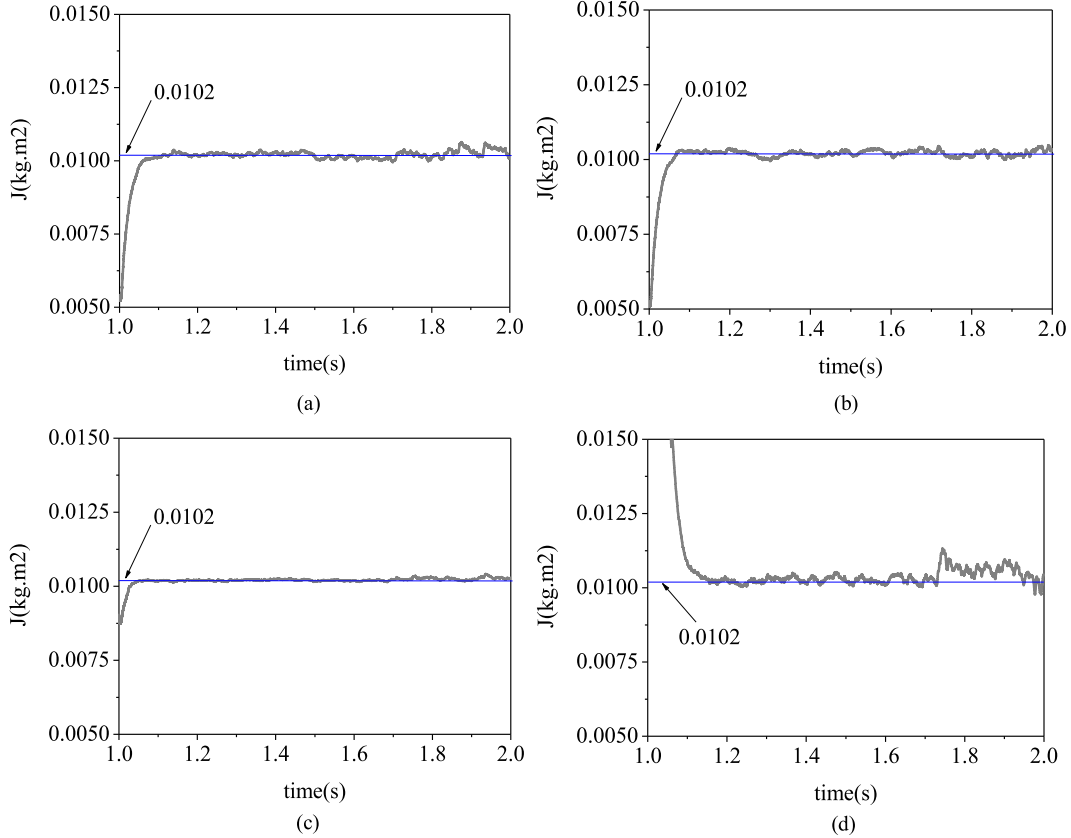


Fig. 14. Experimental results of estimated J . (a) $J_0 = 0.001 J$. (b) $J_0 = 0.01 J$. (c) $J_0 = 2.5 J$. (d) $J_0 = 10 J$.

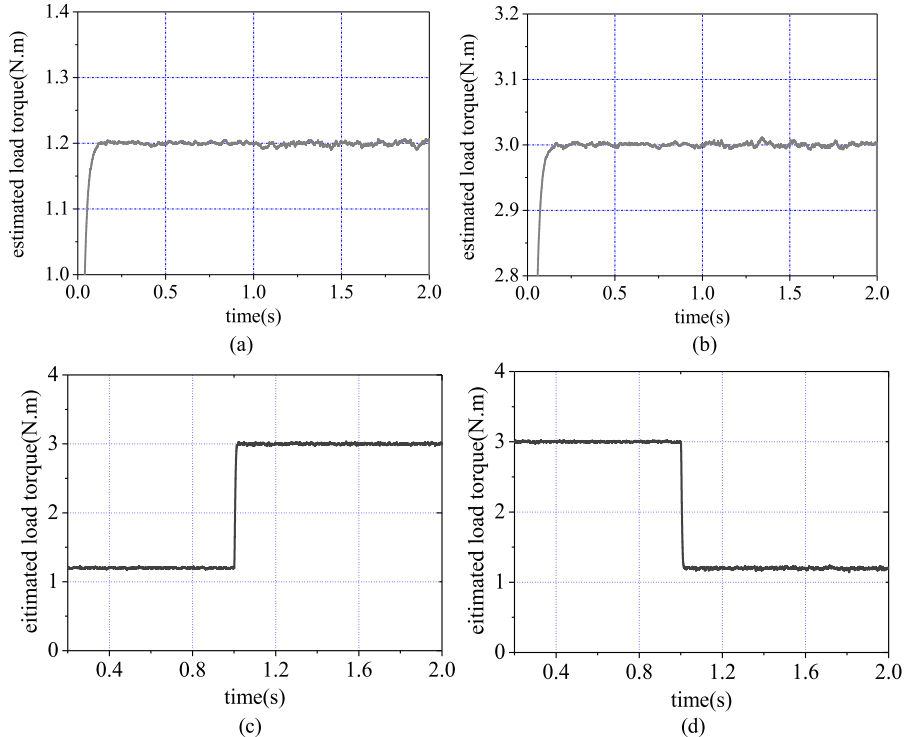


Fig. 15. Experimental results of estimated T_L . (a) $T_L = 1.2 \text{ N}\cdot\text{m}$. (b) $T_L = 3 \text{ N}\cdot\text{m}$. (c) Estimated load torque in case of sudden load increase from 1.2 to 3 $\text{N}\cdot\text{m}$. (d) Estimated load torque in case of sudden load decrease from 3 to 1.2 $\text{N}\cdot\text{m}$.

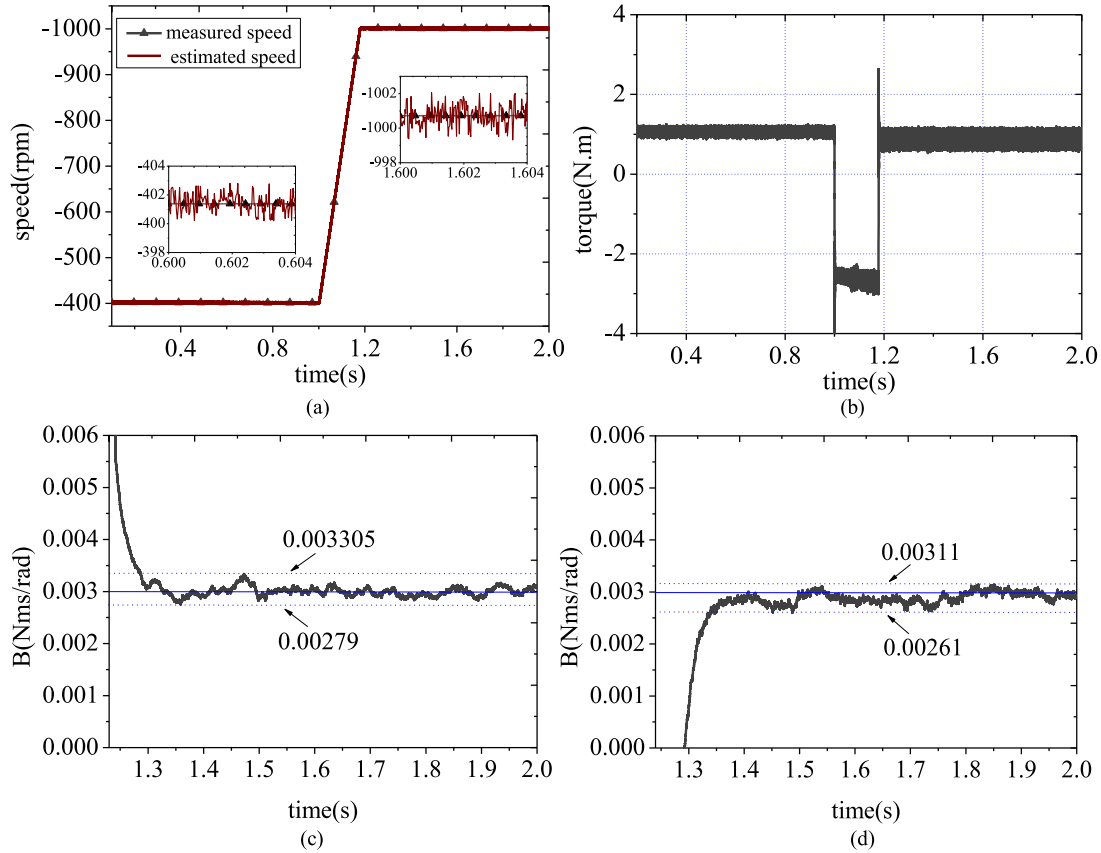


Fig. 16. Experimental results of estimated B under speed reversals. (a) Measured speed and estimated speed. (b) Torque. (c) $B_0 = 0.0001 B$. (d) $B_0 = 50 B$.

The experimental measurements of the motor speed, the driving torque, and the estimated disturbance are shown in Fig. 11 when the parameter B is estimated. Fig. 12 shows the experimental measurements of the motor speed, the driving torque, and the estimated disturbance when the parameter J is estimated. The mechanical parameter estimation results are shown in Figs. 13–15. The estimation of B is displayed in Fig. 13. There are four different crude estimations of the true parameter of B , i.e., $B_0 = 0.0001 B$, $B_0 = 0.01 B$, $B_0 = 1.33 B$, and $B_0 = 50 B$, corresponding to Fig. 13(a)–(d). It is obvious that all the estimation curves of parameter B converge to the true parameter value. Similarly, Fig. 14 shows the estimations of J with four different crude estimations, i.e., $J_0 = 0.001 J$, $J_0 = 0.01 J$, $J_0 = 2.5 J$, and $J_0 = 10 J$, corresponding to Fig. 14(a)–(d). It can also be found that all the estimation curves of parameter J can converge to the true value. Moreover, the estimation of load torque is shown in Fig. 15(a) and (b) when the load torques $T_L = 1.2 \text{ N}\cdot\text{m}$ and $T_L = 3 \text{ N}\cdot\text{m}$ are added, respectively. Fig. 15(c) shows the dynamic response of estimated torque, when the load torque T_L increases from 1.2 to 3 N·m suddenly. On the other hand, when the load torque T_L decreases from 3 to 1.2 N·m suddenly, the dynamic response of estimated torque is shown in Fig. 15(d). It should be noted that the proposed method can estimate load torque exactly and quickly, which means that estimated load torque can be used to develop disturbance rejection technique in a PMSM control system.

In order to evaluate the performance of the proposed estimator at zero speed and during speed reversals, the experiment results with different speed conditions are shown in Figs. 16–18. There are two different crude estimations of the true parameter of B and J , respectively, i.e., $B_0 = 0.0001 B$, $B_0 = 50 B$, $J_0 = 0.001 J$, and $J_0 = 10 J$, corresponding to Figs. 16(c), (d) and 17(c), (d). The estimations of B with zero speed are displayed in Fig. 18. Fig. 18(a) and (b) shows the speed responses and estimated B when speed changes from 0 to 1200 r/min. Moreover, when speed changes from 0 to $-1200 \text{ r}/\text{min}$, the speed responses and estimated B are shown in Fig. 18(c) and (d). According to experiment results, it can be found that the proposed estimation technique perform well at zero speed and during speed reversals.

The experiment results of parameter estimation with three different cutoff frequency of equivalent LPF, i.e., $m = 2$, $m = 5$ and $m = 10$, are shown in Fig. 19. From the results, it can be seen that the lower cutoff frequency indicates higher performance of parameter estimation. Then, one can adjust the cutoff frequency of an equivalent LPF based on the requirement of chattering suppression in the observer, since the condition (19) is satisfied.

In order to prove the occurrence of sliding mode, the experiment results using estimated speed as speed feedback are displayed in Fig. 20, which shows the estimated speed and measured speed waveforms when speed feedback signal switching from measured speed to estimated speed at 1 s. In addition, PI

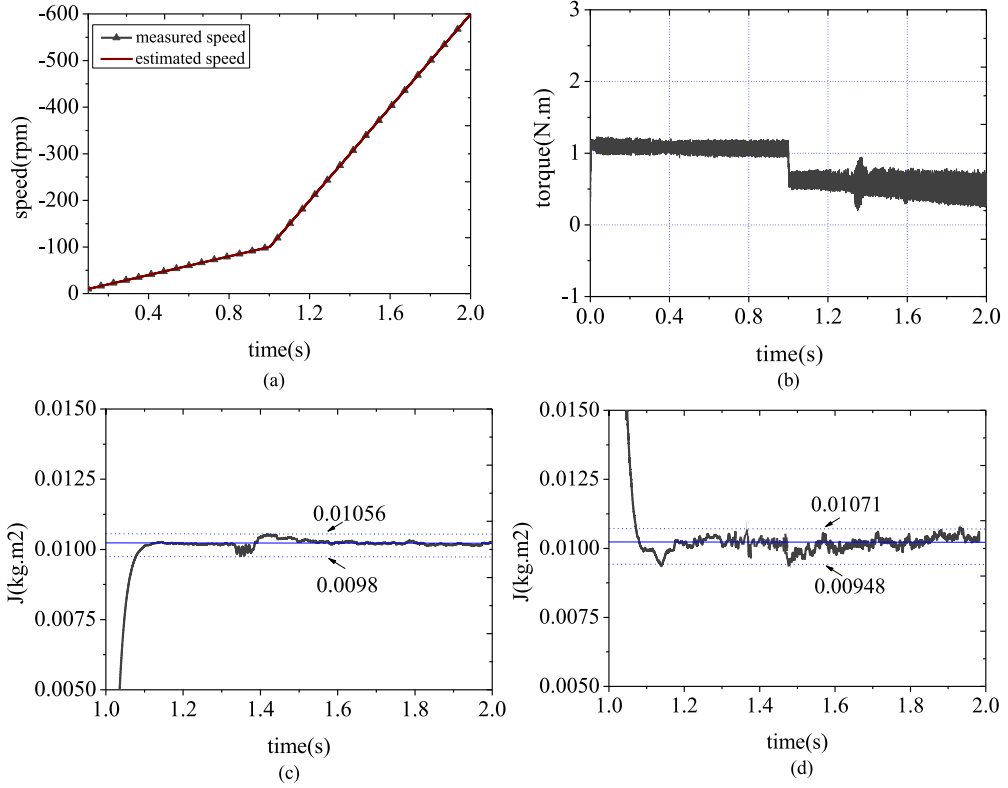


Fig. 17. Experimental results of estimated J under acceleration reversals. (a) Measured speed and estimated speed. (b) Torque. (c) $J_0 = 0.001$ J . (d) $J_0 = 10$ J .

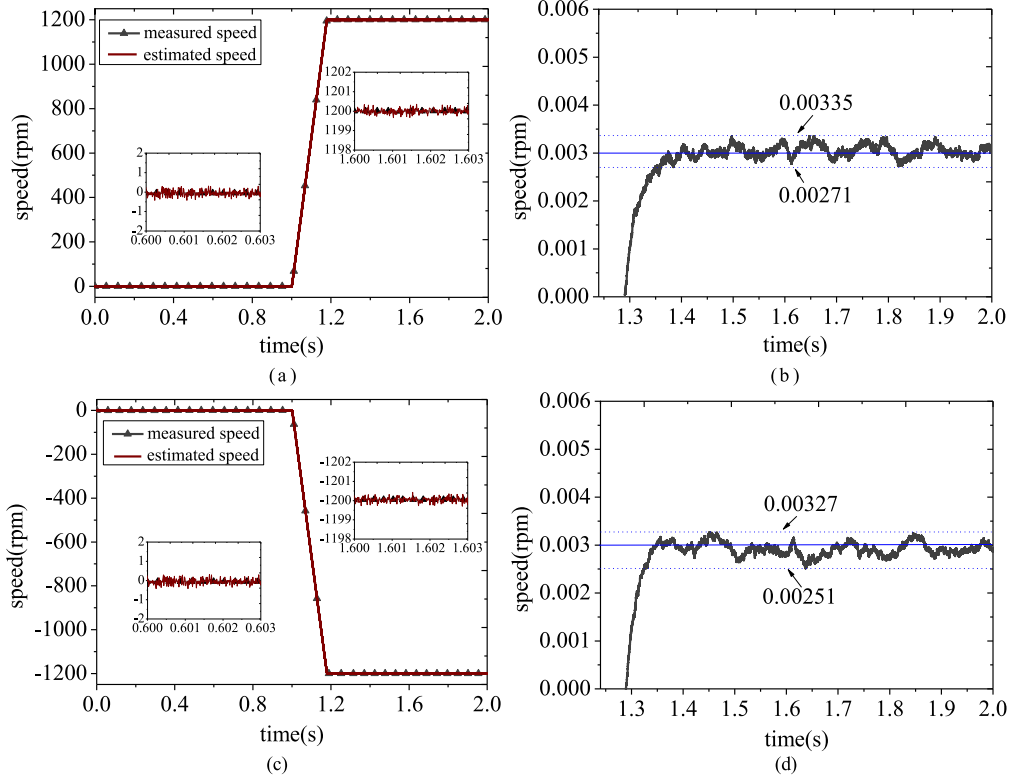


Fig. 18. Experimental results of estimated B at zero speed with $B_0 = 50$ B . (a) Measured speed and estimated speed when speed changes from 0 to 1200 r/min. (b) Estimated B when speed changes from 0 to 1200 r/min. (c) Measured speed and estimated speed when speed changes from 0 to -1200 r/min. (d) Estimated B when speed changes from 0 to -1200 r/min.

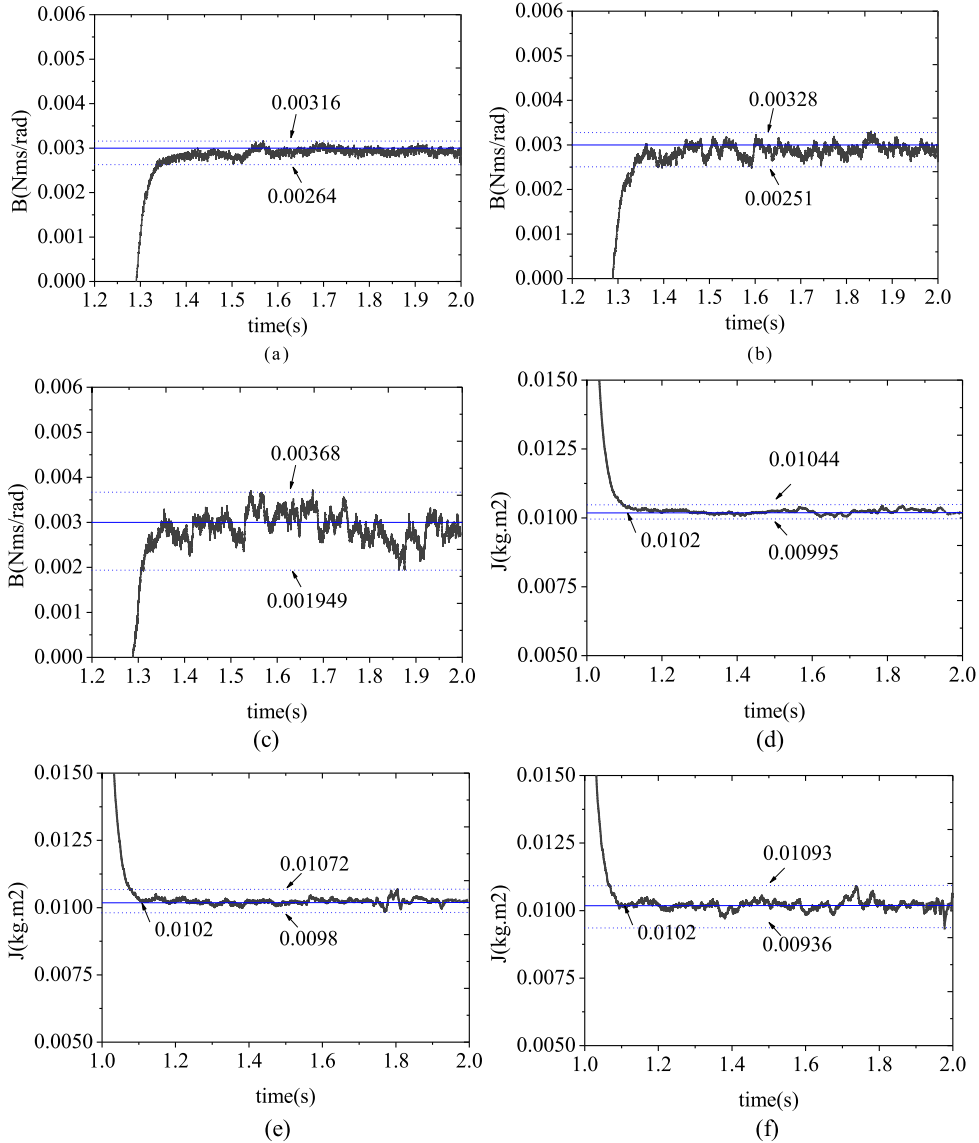


Fig. 19. Experiment results of parameter estimation with three different cutoff frequency of equivalent LPF. (a) Estimated B with $m = 2$, $B_0 = 60$ B . (b) Estimated B with $m = 5$, $B_0 = 60$ B . (c) Estimated B with $m = 10$, $B_0 = 60$ B . (d) Estimated J with $m = 2$, $J_0 = 5$ J . (e) Estimated J with $m = 5$, $J_0 = 5$ J . (f) Estimated J with $m = 10$, $J_0 = 5$ J .

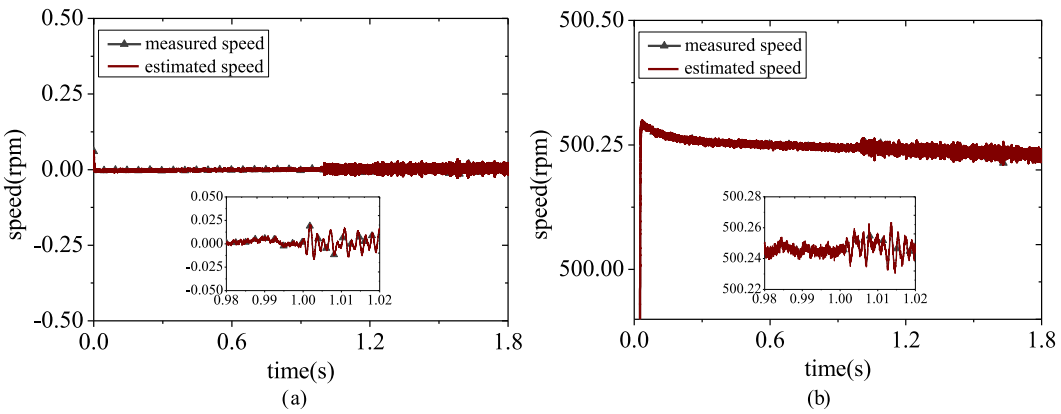


Fig. 20. Experiment results of estimated speed and measured speed when speed feedback signal switching from measured speed to estimated speed at 1 s. (a) Speed response under zero speed. (b) Speed response under 500 r/min.

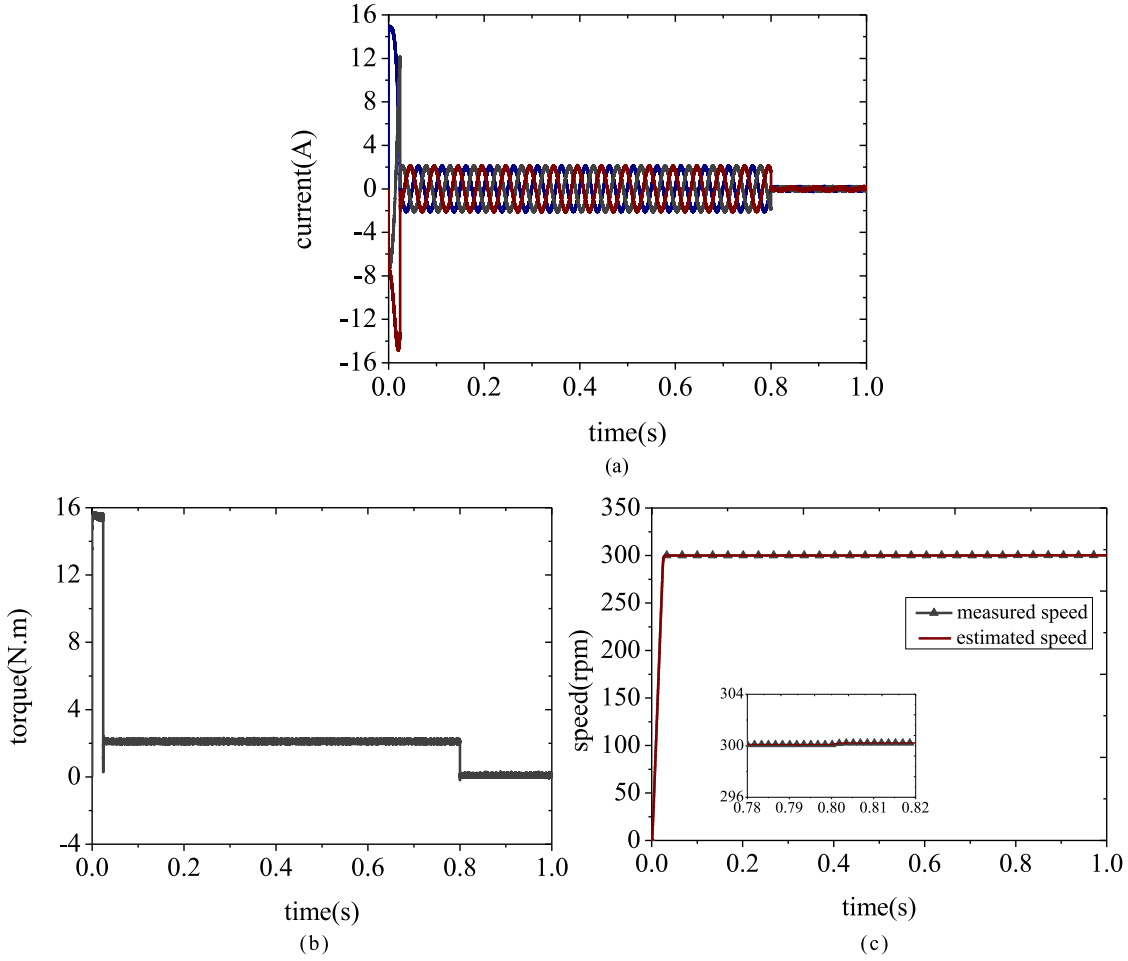


Fig. 21. Experimental results of utilizing estimated parameter in speed controller. (a) Three phase currents. (b) Electromagnetic torque. (c) Speed response.

algorithm is designed as the speed controller, which can be expressed as $G_s = \frac{k_p \cdot s + k_i}{s}$. In this speed PI controller, $k_p = \frac{J \cdot \omega_{sc}^*}{k_t}$ and $k_i = \frac{B \cdot \omega_{sc}^*}{k_t}$ represent proportional gain and integral gain, respectively; $k_t = \frac{3}{2} \Psi_a$ represents torque constant; and ω_{sc}^* is the expected open-loop cutoff frequency of the speed PI controller. Parameters J and B in gain k_p and k_i of speed PI controller can be adjusted using estimated mechanical parameters \hat{J} and \hat{B} based on the proposed observer. The experimental waveforms of utilizing estimated parameter in speed controller are shown in Fig. 21, when load torque suddenly changes from 2 to 0 N·m.

From the experimental results, it is obvious that the estimated parameters can track true values exactly with different crude estimations, speed, and load conditions, which verifies the effectiveness of the proposed estimation method.

VI. CONCLUSION

In this paper, one novel mechanical parameter estimation algorithm is proposed and has been experimentally applied to a PMSM system. The major contributions of this paper include: 1) in order to estimate parameters exactly, one ESMMPO is presented; 2) the equivalent LPF in the ESMMPO can be used to control chattering, which means that the extra LPF can be

avoided and the output signal can be directly used for the parameter estimation; 3) parameter estimation step is designed, which does not need bidirectional rotating operation; and 4) the load torque can be estimated in real time. Experimental results have validated the proposed method.

REFERENCES

- [1] S. Kwak, U.-C. Moon, and J.-C. Park, "Predictive-control-based direct power control with an adaptive parameter identification technique for improved AFE performance," *IEEE Trans. Power Electron.*, vol. 29, no. 11, pp. 6178–6187, Nov. 2014.
- [2] S. Ichikawa, M. Tomita, S. Doki, and S. Okuma, "Sensorless control of permanent-magnet synchronous motors using online parameter identification based on system identification theory," *IEEE Trans. Ind. Electron.*, vol. 53, no. 2, pp. 363–372, Apr. 2006.
- [3] A. Piippo, M. Hinkkanen, and J. Luomi, "Active online system identification of switch mode DC–DC power converter based on efficient recursive DCD-IIR adaptive filter" *IEEE Trans. Power Electron.*, vol. 27, no. 11, pp. 4425–4435, Nov. 2012.
- [4] G. Feng, Y. F. Liu, and L. P. Huang, "Mechanical parameter estimation of motion control systems," *IEEE Trans. Power Electron.*, vol. 19, no. 6, pp. 1614–1627, Nov. 2004.
- [5] L. Liu and D. A. Cartes, "Synchronisation based adaptive parameter identification for permanent magnet synchronous motors," *IET Control Theory Appl.*, vol. 1, no. 4, pp. 1015–1022, Jul. 2007.
- [6] M. Rashed, P. F. MacConnell, and A. Fraser Stronach, "Nonlinear adaptive state-feedback speed control of a voltage fed induction motor with varying

- parameters,” *IEEE Trans. Ind. Appl.*, vol. 42, no. 3, pp. 723–732, May/Jun. 2006.
- [7] T. H. Nguyen and D.-C. Lee, “Deterioration monitoring of DC-link capacitors in AC machine drives by current injection,” *IEEE Trans. Power Electron.*, vol. 30, no. 3, pp. 1126–1130, Mar. 2015.
- [8] Y. He, Y. Wang, Y. Feng, and Z. Wang, “Parameter identification of an induction machine at standstill using the vector constructing method,” *IEEE Trans. Power Electron.*, vol. 27, no. 2, pp. 905–915, Feb. 2012.
- [9] N. Hoffmann and F. W. Fuchs, “Minimal invasive equivalent grid impedance estimation in inductive–resistive power networks using extended Kalman filter,” *IEEE Trans. Power Electron.*, vol. 29, no. 2, pp. 631–641, Feb. 2014.
- [10] H. Renaudineau, J.-P. Martin, B. Nahid-Mobarakeh, and S. Pierfederici, “DC–DC converters dynamic modeling with state observer-based parameter estimation,” *IEEE Trans. Power Electron.*, vol. 30, no. 6, pp. 3356–3363, Jun. 2015.
- [11] K. L. Shi, T. F. Shan, Y. K. Wong, and S. L. Ho, “Speed estimation of an induction motor drive using an optimized extended Kalman filter,” *IEEE Trans. Ind. Electron.*, vol. 49, no. 1, pp. 124–133, Feb. 2002.
- [12] S. Bolognani, L. Tubiana, and M. Zigliotto, “Extended Kalman filter tuning in sensorless PMSM drives,” *IEEE Trans. Ind. Appl.*, vol. 39, no. 6, pp. 1741–1747, Nov./Dec. 2003.
- [13] H. Aung, K. S. Low, and S. Ting Goh, “State-of-charge estimation of lithium-ion battery using square root spherical unscented Kalman filter (SqrUKFST) in nanosatellite,” *IEEE Trans. Power Electron.*, vol. 30, no. 9, pp. 4774–4783, Sep. 2015.
- [14] L. Zhao, J. Huang, H. Liu, and B. Li, “Second-order sliding-mode observer with online parameter identification for sensorless induction motor drives,” *IEEE Trans. Ind. Electron.*, vol. 61, no. 10, pp. 5280–5289, Oct. 2014.
- [15] M.S. Carmeli, F. Castelli-Dezza, M. Iaccetti, and R. Perini, “Effects of mismatched parameters in MRAS sensorless doubly fed induction machine drives,” *IEEE Trans. Power Electron.*, vol. 25, no. 11, pp. 2842–2851, May 2010.
- [16] S. Bolognani, L. Peretti, and M. Zigliotto, “Parameter sensitivity analysis of an improved open-loop speed estimate for induction motor drives,” *IEEE Trans. Power Electron.*, vol. 23, no. 4, pp. 2127–2135, Jul. 2008.
- [17] R. Cárdenas, R. Pena, J. Clare, G. Asher, and J. Proboste, “MRAS observers for sensorless control of doubly-fed induction generators,” *IEEE Trans. Power Electron.*, vol. 23, no. 3, pp. 1075–1084, May 2008.
- [18] F. C. Dezza, G. Foglia, M. F. Iaccetti, and R. Perini, “An MRAS observer for sensorless DFIM drives with direct estimation of the torque and flux rotor current components,” *IEEE Trans. Power Electron.*, vol. 27, no. 5, pp. 2576–2584, May 2012.
- [19] Y. Feng, X. Yu, and F. Hani, “High-order terminal sliding-mode observer for parameter estimation of a permanent-magnet synchronous motor,” *IEEE Trans. Ind. Electron.*, vol. 60, no. 10, pp. 4272–4380, Oct. 2013.
- [20] K. Fujita and K. Sado, “Instantaneous speed detection with parameter identification for ac servo system,” *IEEE Trans. Ind. Appl.*, vol. 28, no. 4, pp. 864–872, Jul. 1992.
- [21] I. Awaya, Y. Kato, I. Miyake, and M. Ito, “New motion control with inertia identification function using disturbance observer,” in *Proc. Power Electron. Motion Control Conf.*, 1992, pp. 77–81.
- [22] J. W. Choi, S. C. Lee, and H. G. Kim, “Inertia identification algorithm for high-performance speed control of electric motors,” in *Proc. Inst. Electr. Eng. Electr. Power Appl.*, vol. 153, no. 3, pp. 379–386, May 2006.
- [23] S. M. Yang and Y. J. Deng, “Observer-based inertia identification for auto tuning servo motor drives,” in *Proc. IEEE Conf. Rec. 40th Ind. Appl. Annu. Meet.*, 2005, pp. 968–972.
- [24] S. Yang and Y. Deng, “Observer-based inertial identification for autotuning servo motor drives,” in *Proc. IEEE Conf. Rec. Ind. Appl. Annu. Meet.*, Hong Kong, Oct. 2–6, 2005, vol. 2, pp. 968–972.
- [25] J. Davila, L. Fridman, and A. Poznyak, “Observation and identification of mechanical systems via second order sliding modes,” *Int. J. Control.*, vol. 79, no. 10, pp. 1251–1262, Oct. 2006.
- [26] J. Davila, L. Fridman, and A. Levant, “Second-order sliding-mode observer for mechanical systems,” *IEEE Trans. Autom. Control*, vol. 50, no. 11, pp. 1785–1789, Nov. 2005.
- [27] Z. Kan Liu, Q. Zhu, Q. Zhang, and J. Zhang, “Influence of nonideal voltage measurement on parameter estimation in permanent-magnet synchronous machines,” *IEEE Trans. Ind. Electron.*, vol. 59, no. 6, pp. 2438–2447, Jun. 2012.



Xiaoguang Zhang was born in Heilongjiang, China, in 1985. He received the B.S. degree in electrical engineering from the Heilongjiang Institute of Technology, Harbin, China, in 2007, and the M.S. and Ph.D. degrees in electrical engineering from the Harbin Institute of Technology, Harbin, in 2009 and 2014, respectively.

He is currently an Assistant Professor at the North China University of Technology, Beijing, China. From 2012 to 2013, he was a Research Associate with Wisconsin Electric Machines and Power Electronics Consortium, University of Wisconsin-Madison, Madison, WI, USA. His research interest includes electric machines and drives.



Zhengxi Li (SM’07) received the B.S., Master’s, and Ph.D. degrees from the University of Science and Technology, Beijing, China, in 1984, 1990, and 2004, respectively, all in control science and engineering.

He is currently a Professor of electrical engineering and the Vice President of the North China University of Technology, Beijing. His research interests include motor drives and intelligent transportation.